THE JOURNAL OF BIOLOGICAL CHEMISTRY VOL. 291, NO. 15, pp. 8048–8058, April 8, 2016

Non-lysosomal Degradation of Singly Phosphorylated Oligosaccharides Initiated by the Action of a Cytosolic Endo-β-*N*-acetylglucosaminidase*

Received for publication, August 13, 2015, and in revised form, January 28, 2016 Published, JBC Papers in Press, February 8, 2016, DOI 10.1074/jbc.M115.685313

Yoichiro Harada[‡1], **Chengcheng Huang**[‡], **Satoshi Yamaki**[§], **Naoshi Dohmae**[¶], **and Tadashi Suzuki**[‡2]

From the [‡]*Glycometabolome Team, Systems Glycobiology Research Group, RIKEN-Max Planck Joint Research Center, Global Research Cluster, RIKEN, 2-1 Hirosawa, Wako, Saitama 351-0198, the* [§]*Global Application Development Center, Analytical and Measuring Instruments Division, Shimadzu Corp., Hadano, Kanagawa 259-1304, and the* [¶]*Collaboration Promotion Unit, RIKEN Global Research Cluster, Wako, Saitama 351-0198, Japan*

Phosphorylated oligosaccharides (POSs) are produced by the degradation of dolichol-linked oligosaccharides (DLOs) by an unclarified mechanism in mammalian cells. Although POSs are exclusively found in the cytosol, their intracellular fates remain unclear. Our findings indicate that POSs are catabolized via a non-lysosomal glycan degradation pathway that involves a cytosolic endo-β-*N*-acetylglucosaminidase (ENGase). Quantitative and structural analyses of POSs revealed that ablation of the ENGase results in the significant accumulation of POSs with a hexasaccharide structure composed of Manα1,2Manα1,3(Manα1,6)Manβ1,4GlcNAcβ1,4GlcNAc. *In vitro* ENGase assays revealed that the presence of an α1,2-linked mannose residue facilitates the hydrolysis of POSs by the ENGase. Liquid chromatography-mass spectrometric analyses and fluorescent labeling experiments show that such POSs contain one phosphate group at the reducing end. These results indicate that ENGase efficiently hydrolyzes POSs that are larger than $Man_4GlcNAc_2$-P, generating GlcNAc-1-P and neutral Gn1-type free oligosaccharides. These results provide insight into important aspects of the generation and degradation of POSs.

Dolichol-linked oligosaccharides (DLOs)[3] are glycan donor substrates for asparagine (*N*)-linked glycosylation in mammals (1, 2). The biosynthesis of DLOs starts on the cytosolic side of the endoplasmic reticulum (ER) membrane with the assembly of $Man_5GlcNAc_2$-PP-Dol (1). This biosynthetic intermediate is flipped into the ER lumen and is converted to $Glc_3Man_9GlcNAc_2$-PP-Dol. The fully assembled DLO is then transferred onto nascent polypeptides by the oligosaccharyltransferase (3).

In mammalian cells, the biosynthesis of DLOs is regulated by the supply of glucose. When cells are deprived of glucose, incompletely assembled DLOs are produced (4–9), which are rapidly degraded by a currently unclarified degradation system (2, 10, 11). The enzyme involved in the degradation has long been believed to hydrolyze the pyrophosphate bond of DLOs, releasing phosphorylated oligosaccharides (POSs) into the cytosol (Fig. 1, *step i*) (10–14). Although previous biochemical studies using paper electrophoresis (11) or anion-exchange chromatography (10, 14) suggest the presence of one phosphate group on POSs, the precise number has not been unequivocally determined, which has hampered the identification of the precise action of the DLO-degrading enzyme.

In addition to POSs, a protein-unbound form of neutral high mannose-type *N*-glycans (free *N*-glycans; FNGs), which bare *N*,*N*′-diacetylchitobiose at the reducing end (Gn2-type), is produced in the cytosol via two distinct pathways as follows: the degradation of DLOs, presumably by oligosaccharyltransferase in the ER lumen (2, 15, 16), and their transport to the cytosol (Fig. 1, *step ii*); and the deglycosylation of misfolded glycoproteins by a cytosolic peptide:*N*-glycanase (PNGase) (Fig. 1, *step iii*) (2, 17, 18). In the cytosol, the Gn2-type FNGs are processed by an endo-β-*N*-acetylglucosaminidase (ENGase) (19–21) that hydrolyzes the innermost GlcNAc residue to generate Gn1-type FNGs (Fig. 1, *step iv*). The action of ENGase is prerequisite for the subsequent trimming of mannose from the FNGs by the α-mannosidase Man2C1 (Fig. 1, *step v*) (21, 22). This process, which is referred to as non-lysosomal glycan degradation, accelerates the transport of FNGs into lysosomes and their subsequent degradation (Fig. 1, *step vi*) (23). Although the molecular mechanism responsible for how POSs are catabolized remains unclear, it has been suggested that POSs predominantly accumulate in the cytosol (10, 13, 14).

In this study, we investigated the issue of whether cytosolic ENGase catalyzes the hydrolysis of POSs (Fig. 1, *step vii*), because an *N*,*N*′-diacetylchitobiose core structure is still intact at their reducing ends. Structural analyses of POSs by liquid chromatography-mass spectrometry (LC-MS) showed that the reducing end of the POSs is mono-phosphorylated. Comparisons of POSs produced in wild-type and *Engase* knock-out ($Engase^{-/-}$) mouse embryonic fibroblasts (MEFs) revealed that POSs that carry Manα1,2Manα1,3(Manα1,6)Manβ1,4GlcNAcβ1,4GlcNAc accumulate to a significant extent in $Engase^{-/-}$ MEFs. Consistent with this observation, *in vitro* ENGase assays for POSs with various structures clearly indi-

* This work was supported in part by Grants-in-aid from the Ministry of Education, Culture, Sports, Science, and Technology of Japan 24770134 and 26650040 (to Y. H.) and 25291030 (to T. S.). The authors declare that they have no conflicts of interest with the contents of this article.

[1] Present address: Dept. of Systems Biology in Thromboregulation, Kagoshima University Graduate School of Medical and Dental Sciences, Sakuragaoka, Kagoshima 890-8544, Japan.

[2] To whom correspondence should be addressed. Tel.: 81-48-467-9628; Fax: 81-48-467-9626; E-mail: tsuzuki_gm@riken.jp.

[3] The abbreviations used are: DLO, dolichol-linked oligosaccharide; POS, phosphorylated oligosaccharide; ENGase, endo-β-*N*-acetylglucosaminidase; MEF, mouse embryonic fibroblast; ER, endoplasmic reticulum; FNG, free *N*-glycan; PA, 2-aminopyridine; CIP, calf intestine alkaline phosphatase; Endo, endoglycosidase.

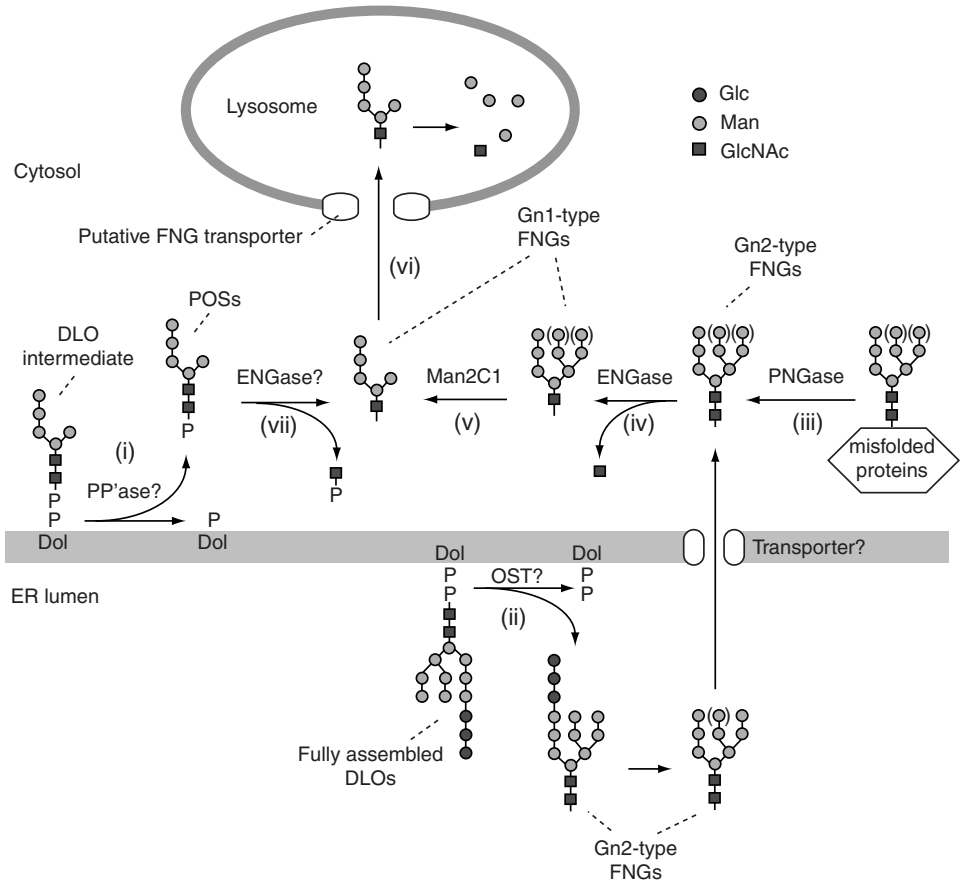

FIGURE 1. **Model of the generation and the non-lysosomal degradation of FNGs and POSs in mammalian cells (2, 35).** Biosynthetic intermediates of DLOs, *e.g.* $Man_5GlcNAc_2$-PP-Dol, are presumably degraded by a putative pyrophosphatase (*PP'ase*), releasing POSs into the cytosol (*step i*). In the cytosol, Gn2-type FNGs are generated by either the degradation of the fully assembled DLO, presumably by oligosaccharyltransferase (*step ii*) or the deglycosylation of misfolded glycoproteins by PNGase (*step iii*). ENGase hydrolyzes the Gn2-type FNGs to produce Gn1-type FNGs and free GlcNAc (*step iv*). The action of ENGase facilitates mannose trimming of the Gn1-type FNGs by Man2C1 (*step v*) and lysosomal transport of the FNGs via unidentified FNG transporter (*step vi*). Although the POSs are not readily transported into lysosomes, the removal of the phosphate group from a POS can initiate the lysosomal transport of the resultant FNGs (23). The hydrolysis of POSs by ENGase may facilitate the catabolism of POSs by removing GlcNAc-P from POSs (*step vii*).

cated that this enzyme preferentially hydrolyzes POSs that contain an α1,2-linked mannose residue. These results strongly indicate that ENGase efficiently catabolizes POSs that are larger than $Man_4GlcNAc_2$-P and generates Gn1-type FNGs and GlcNAc-1-P in the cytosol.

Experimental Procedures

Establishment of MEFs—Wild-type, *Engase*$^{-/-}$, and *Ngly1*$^{-/-}$ *Engase*$^{-/-}$ MEFs were established and immortalized as described previously (24).

Cell Culture—MEFs (2×10^6 cells/15-cm dish) were seeded and incubated for 24 h at 37 °C in 20 ml of complete Dulbecco's modified Eagle's medium (DMEM), high glucose (Nakalai) supplemented with 10% (v/v) FBS, 100 units/ml penicillin, and 100 μg/ml streptomycin in a 5% CO_2 atmosphere. Cells were washed twice with 10 ml of DMEM without glucose (Invitrogen) and then further incubated for 24 h at 37 °C in 20 ml of DMEM without glucose supplemented with either 5 mM (normal glucose condition) or 0.5 mM (low glucose condition) glucose, 10% (v/v) FBS, 100 units/ml penicillin, and 100 μg/ml streptomycin.

Preparation of POSs from MEFs—POSs were prepared essentially as described in a previous report (10). Briefly, MEFs were extracted with 70% (v/v) ethanol, and the soluble fraction was evaporated to dryness. The dried pellet was dissolved in 2.5 ml of water and desalted by passage through a PD-10 column (GE Healthcare) equilibrated with 5% (v/v) ethanol. The desalted sample was adjusted to 10 mM Tris-HCl, pH 7.4, and subjected to anion-exchange column chromatography using a Sep-Pak Accell QMA column (Waters). POSs were eluted from the anion-exchange column with 5 ml of an elution buffer containing 10 mM Tris-HCl, pH 7.4, and 70 mM NaCl.

For the analysis of POSs by LC-MS, the eluates from the anion-exchange column were desalted on PD-10 columns equilibrated with 5% (v/v) ethanol, followed by passing through a 250-μl CM-Sepharose (GE Healthcare) equilibrated with water. The flow-through fraction, which contains POSs, was evaporated to dryness and dissolved in a small volume of water and then subjected to LC-MS analysis.

Pyridylamination—POSs eluted from the anion-exchange chromatography column were dephosphorylated by treatment with recombinant calf intestine alkaline phosphatase (CIP; 1 unit, Roche Applied Science) for 16 h at 37 °C. The dephosphorylated POSs were desalted on an InertSep GC column (150 mg/3 ml; GL Sciences), evaporated to dryness,

TABLE 1
Yeast strains used in this study and the major glycan structures of their DLOs

Name / Genotypes	Major glycan structures of DLOs[a]	Source
Wild-type *MATα his3Δ1 leu2Δ0 met15Δ0 ura3Δ0 BY4741*	Manα1-2Manα1 6 Manα1 3 Manα1-2Manα1 6 Manβ1-4GlcNAcβ1-4GlcNAc 3 Glcα1-3Glcα1-2Glcα1-2Manα1-2Manα1-2Manα1	Open Biosystems
alg6Δ *MATα his3Δ1 leu2Δ0 met15Δ0 ura3Δ0 alg6Δ::kanMX4 BY4741*	Manα1-2Manα1 6 Manα1 3 Manα1-2Manα1 6 Manβ1-4GlcNAcβ1-4GlcNAc 3 Manα1-2Manα1-2Manα1	Open Biosystems
alg3Δ *MATα his3Δ1 leu2Δ0 met15Δ0 ura3Δ0 alg3Δ::kanMX4 BY4741*	Manα1 6 Manβ1-4GlcNAcβ1-4GlcNAc 3 Manα1-2Manα1-2Manα1	Open Biosystems
alg11Δ *MATα his3Δ1 leu2Δ0 met15Δ0 ura3Δ0 alg11Δ::His3MX6 BY4741*	Manα1 6 Manβ1-4GlcNAcβ1-4GlcNAc 3 Manα1	This study

[a] Major glycan structures of DLOs from wild-type (41), *alg6*Δ (36), *alg3*Δ (37), and *alg11*Δ (38–40) cells were deduced based on the previous reports.

and labeled with 2-aminopyridine (PA) as described previously (15).

High Performance Liquid Chromatography (HPLC)—Size fractionation HPLC (15) and dual-gradient reversed-phase HPLC (25) were carried out as described previously. PA-glycans were quantitated using PA-Glc_6 that is included in PA-glucose oligomer (Takara; 2 pmol/μl) as an external standard.

Preparation of Standard PA-labeled Oligosaccharides—Standard PA-labeled oligosaccharides (PA-Gn2, PA-M1A, PA-M4D, PA-M5B, PA-M6E, and PA-M7E) were prepared as described previously (10). PA-M2A, PA-M3B, PA-M8C, and PA-M9A were purchased from Takara.

LC-MS of POSs—POSs (17 pmol as $Man_2GlcNAc_2$-P) obtained from the glucose-deprived wild-type MEFs (10) were analyzed by LC-MS using a quadrupole ion trap time-of-flight mass spectrometer (LCMS-IT-TOF, Shimadzu Corp.) in electrospray ionization (ESI) in the negative ion mode. For analysis, 10-μl aliquots (maintained at 4 °C in the auto sampler) were injected for separation by HPLC, using gradient elution, with a Nexera XR LC system (Shimadzu Corp.) on a Mastro C18 column (100 × 2.1 mm; particle size 3.0 μm) at a flow rate of 0.3 ml min^{-1}, with the column maintained at 40 °C. The chromatographic system used a binary solvent system delivered as a gradient of Solvent A (15 mM ammonium acetate, 10 mM tributylamine solution) and Solvent B (methanol). The initial gradient conditions were 100% A, 0% B for 0.5 min followed by a linear gradient up to 25% B in 8 min, and up to 98% B over the next 4 min. The solvent composition was then held at 98% B for 3 min after which the column was returned to 0% B over the next 5 min, making a total cycle time of 20 min per sample. The following method parameters were used for sample analysis: mass range of m/z 200–1500 in MS; ion source temperature of 200 °C; heated capillary temperature of 200 °C; electrospray voltage of −3.5 kV; electrospray nebulization gas flow 1.5 liters/min; detector voltage 1.7 kV; ion accumulation time 30 ms.

The negative ion mode was used. Mass calibration was carried out using a trifluoroacetic acid sodium solution (2.5 mmol $liter^{-1}$) from 200 to 1500 Da. Data acquisition and processing used software LCMS Solution 3.80.

To verify component identification, the Formula Predictor software was used (Shimadzu Corp.). Predicting a candidate list based on MS data takes into account a number of variables, including isotopic profile analysis, mass accuracy, and mass resolution of the experimentally derived pseudomolecular ion peak and related fragment ion data.

Large Scale Preparation of the DLOs—Saccharomyces cerevisiae strains used to prepare DLOs are listed in Table 1. Wild-type, *alg6*Δ, and *alg3*Δ cells were transformed with pRS425-GPD-ALG7 to overproduce DLOs (15). The transformants were grown in complete synthetic medium without leucine (26). In contrast, *alg11*Δ cells were grown in YPD medium (1% yeast extract, 2% polypeptone, 2% glucose). The DLOs were prepared from those strains, and their amounts were quantitated as described previously (15).

Preparation of Detergent-solubilized Mouse Liver Microsomes—Microsomes were prepared from livers of C57BL/6 mice as described previously (27), except that 30% (v/v) glycerol was used instead of 1.3 M sucrose as a cushion to sediment the rough ER by ultracentrifugation. Mouse liver microsomes obtained were homogenized in a homogenization buffer containing 20 mM Hepes-KOH, pH 7.4, 150 mM KCl, 5 mM $CoCl_2$, and 1% (w/v) Triton X-100 and ultracentrifuged at 100,000 × *g* for 20 min. The supernatant was recovered as detergent-solubilized microsomes. All experimental protocols and procedures were approved by the Ethical Committees on Animal Research of RIKEN.

In Vitro DLO-Pyrophosphatase Assay—DLOs (4 nmol) were dissolved in 25 μl of homogenization buffer and incubated for 16 h at 37 °C with 25 μl of detergent-solubilized microsomes supplemented with glycosidase inhibitors (10 μM swainsonine, 100 μM kifunensine, and 1 mM castanospermine). The reaction was terminated by the addition of 3 volumes of ethanol. After centrifugation at 15,000 × *g* for 10 min, the supernatant was evaporated to dryness. POSs were purified from the dried pellet and desalted as described above under "Preparation of POSs from MEFs."

Transfection—Ngly1$^{-/-}$ *Engase*$^{-/-}$ MEFs (1.0×10^6 cells) were seeded to a 10-cm dish and incubated in 10 ml of complete DMEM without antibiotics for 24 h before transfection. The cells were transfected with 1 μg of pcDNA3.1-mouse ENGase-FLAG (24) using 5 μl of Lipofectamine 2000 (Thermo Fischer Scientific). At 16 h after transfection, the cells were harvested, and the cytosolic fraction was prepared.

Preparation of the Cytosolic Fraction—Ngly1$^{-/-}$ *Engase*$^{-/-}$ MEFs overexpressing mouse ENGase were washed three times with ice-cold phosphate-buffered saline. The cells obtained from a 10-cm dish were homogenized in 300 μl of cytosol extraction buffer containing 10 mM Hepes-NaOH, pH 7.4, 250 mM mannitol, 5 mM dithiothreitol, 1 mM EDTA, 1× complete protease inhibitor mixture (EDTA-free, Roche Applied Science), and 1 mM Pefabloc (Roche Applied Science). The homogenate was centrifuged at 10,000 × *g* for 10 min at 4 °C. The supernatant was further ultracentrifuged at 100,000 × *g* for 60 min at 4 °C to remove the microsomal fraction, and the supernatant was recovered as the cytosol fraction.

To remove endogenous FNGs, the cytosol fraction (400 μl) was concentrated to ~50 μl using an Amicon Ultra MWCO 50-kDa filter (Millipore) by centrifugation at 10,000 × *g* for 6 min at 4 °C and diluted with 450 μl of cytosol extraction buffer. After the dilution-concentration step was carried out twice, the final concentrate (~ 100 μl) was recovered, aliquoted, flash-frozen in liquid nitrogen, and stored at −80 °C until used.

ENGase Activity Assay—The ultrafiltrated cytosol fraction (20 μl) was incubated with 30 μl of ENGase reaction buffer containing 50 pmol of POSs, 50 mM MES-NaOH, pH 6.0, and glycosidase inhibitors (final concentration: 10 μM swainsonine, 100 μM kifunensine, and 1 mM castanospermine) for 1, 2, and 4 h (for $Glc_3Man_9GlcNAc_2$-P, $Man_9GlcNAc_2$-P, and $Man_5GlcNAc_2$-P) or 2, 4, and 8 h (for $Man_3GlcNAc_2$-P) at 30 °C. For control, $Man_5GlcNAc_2$-P was incubated with the ultrafiltrated cytosol fraction without ENGase overexpression for 2 h at 30 °C. The reaction was terminated by the addition of 300 μl of 75% (v/v) ethanol and incubated for 15 min at 0 °C. After centrifugation at 15,000 × *g* for 10 min at 4 °C, the supernatant was evaporated to dryness. The resulting sample was dissolved in water, desalted on an ion-exchange column containing a stack of AG50-X8 (250 μl, 200–400 mesh, H^+ form) and AG1-X2 (250 μl, 200–400 mesh, acetate form) (Bio-Rad), followed by an InertSep GC column (150 mg/3 ml) (GL Sciences). The desalted glycans were fluorescently labeled as described above under "Pyridylamination."

Fluorescently labeled glycans were analyzed by size-fractionation HPLC. For the detection of PA-labeled $Man_9GlcNAc_1$ and $Man_5GlcNAc_1$, details for the HPLC condition were described previously (28). For the detection of PA-labeled $Glc_3Man_9GlcNAc_1$ and $Man_3GlcNAc_1$, the following HPLC conditions were used: eluent A, 93% acetonitrile in 0.3% acetate buffer (pH 7.0 adjusted by ammonia); eluent B, 20% acetonitrile in 0.3% acetate buffer (pH 7.0 adjusted by ammonia). The column temperature was 25 °C. The flow rate was 0.8 ml/min. The gradient program was as follows: 0–0.5 min, 1–10% eluent B; 0.5–45 min, 10–55% eluent B; 45–47 min, isocratic 70% eluent B; 47–67 min, isocratic 1% eluent B.

Endoglycosidase Digestion of POSs—To verify the elution positions of Gn1-type FNGs in dual-gradient reversed-phase HPLC (25), POSs (50 pmol) that were obtained as described above under "In Vitro DLO-Pyrophosphatase Assay" were digested with either Endo-H (for $Glc_3Man_9GlcNAc_2$-P and $Man_9GlcNAc_2$-P; Roche Applied Science, 5 milliunits) or Endo-M (for $Man_5GlcNAc_2$-P and $Man_3GlcNAc_2$-P; Tokyo Chemical Industry, 1 milliunit) in 30 μl of ENGase reaction buffer at 37 °C for 4 h. The reaction was terminated by the addition of 300 μl of 75% (v/v) ethanol, desalted, and fluorescently labeled as described above under "ENGase Activity Assay."

Results

POSs Are Mono-phosphorylated—To unequivocally determine the number of phosphate groups of the POSs, POSs that were produced in glucose-deprived wild-type MEFs (10) were analyzed by reversed-phase LC-ESI-MS. In the negative ion mode, singly charged deprotonated molecules $[M - H]^-$ corresponding to $HexNAc_2$-P (*m/z* 503.1285), $Hex_1HexNAc_2$-P (*m/z* 665.1806), $Hex_2HexNAc_2$-P (*m/z* 827.2333), $Hex_3HexNAc_2$-P (*m/z* 989.2844), $Hex_4HexNAc_2$-P (*m/z* 1151.3464), and $Hex_5HexNAc_2$-P (*m/z* 1313.3931) were eluted at around 6.3, 6.0, 5.8, 5.5, 5.1, and 4.9 min in reversed-phase HPLC (Fig. 2). However, no doubly charged deprotonated molecules $[M - 2H]^{2-}$ corresponding to diphosphorylated POSs were detected. These results clearly show that the POSs were mainly monophosphorylated, consistent with the predictions made by previous biochemical studies (10, 11, 14).

Ablation of Engase Results in the Accumulation of POSs That Are Larger than Manα1,2Manα1,3(Manα1,6)Manβ1,4GlcNAcβ1,4GlcNAc-P—Because ENGase catalyzes the hydrolysis of β1,4-linkage of the *N,N′*-diacetylchitobiose core of protein-bound (24) and unbound (19, 21) forms of high mannose-type glycans in the cytosol of mammalian cells, we speculated that POSs, which are exclusively localized in the cytosol (10, 13, 14), may also serve as physiological substrates for ENGase. To

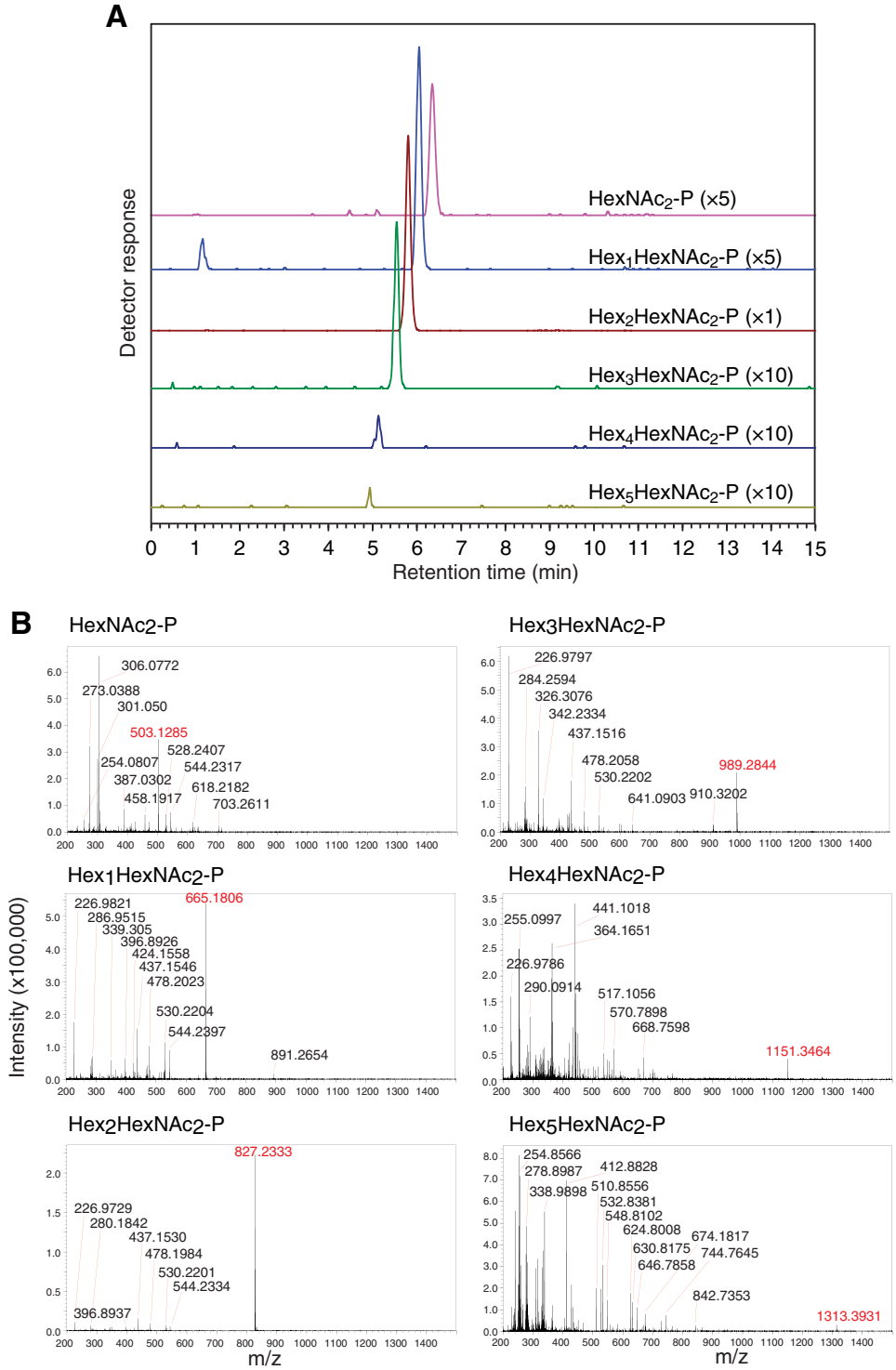

FIGURE 2. **POSs are mono-phosphorylated.** Intact POSs (17 pmol as $Man_2GlcNAc_2$-P) prepared from glucose-deprived wild-type MEFs were analyzed by LC-ESI-MS. *A,* MS chromatograms of $Hex_{0-5}HexNAc_2$-P. *Parentheses* indicate magnification ratio. *B,* MS spectra of $HexNAc_2$-P (*m/z* 503.1285), $Hex_1HexNAc_2$-P (*m/z* 665.1806), $Hex_2HexNAc_2$-P (*m/z* 827.2333), $Hex_3HexNAc_2$-P (*m/z* 989.2844), $Hex_4HexNAc_2$-P (*m/z* 1151.3464), and $Hex_5HexNAc_2$-P (*m/z* 1313.3931). The average mass error for all detected POSs was 0.38 ppm, except that the mass error for $Hex_5HexNAc_2$-P was 5.82 ppm. Typical mass accuracy in external calibration was less than 5 ppm.

test this hypothesis, the amounts and glycan structures of the POSs were compared between wild-type and *Engase*$^{-/-}$ MEFs. The rationale behind this experiment is that if ENGase hydrolyzes POSs, the knock-out of *Engase* would result in the accumulation of POSs. To detect POSs by a conventional fluorescent labeling method for the reducing end of glycans (29), POSs prepared from glucose-deprived MEFs were treated with or without CIP, fluorescently labeled, and separated by size-fractionation HPLC (Fig. 3*A*) (10). Fluorescently labeled glycans that appeared in a dephosphorylation-dependent manner (Fig. 3*A*, *peaks a–h*) were regarded as POSs. The fluorescently labeled POS-derived glycans thus obtained were fractionated

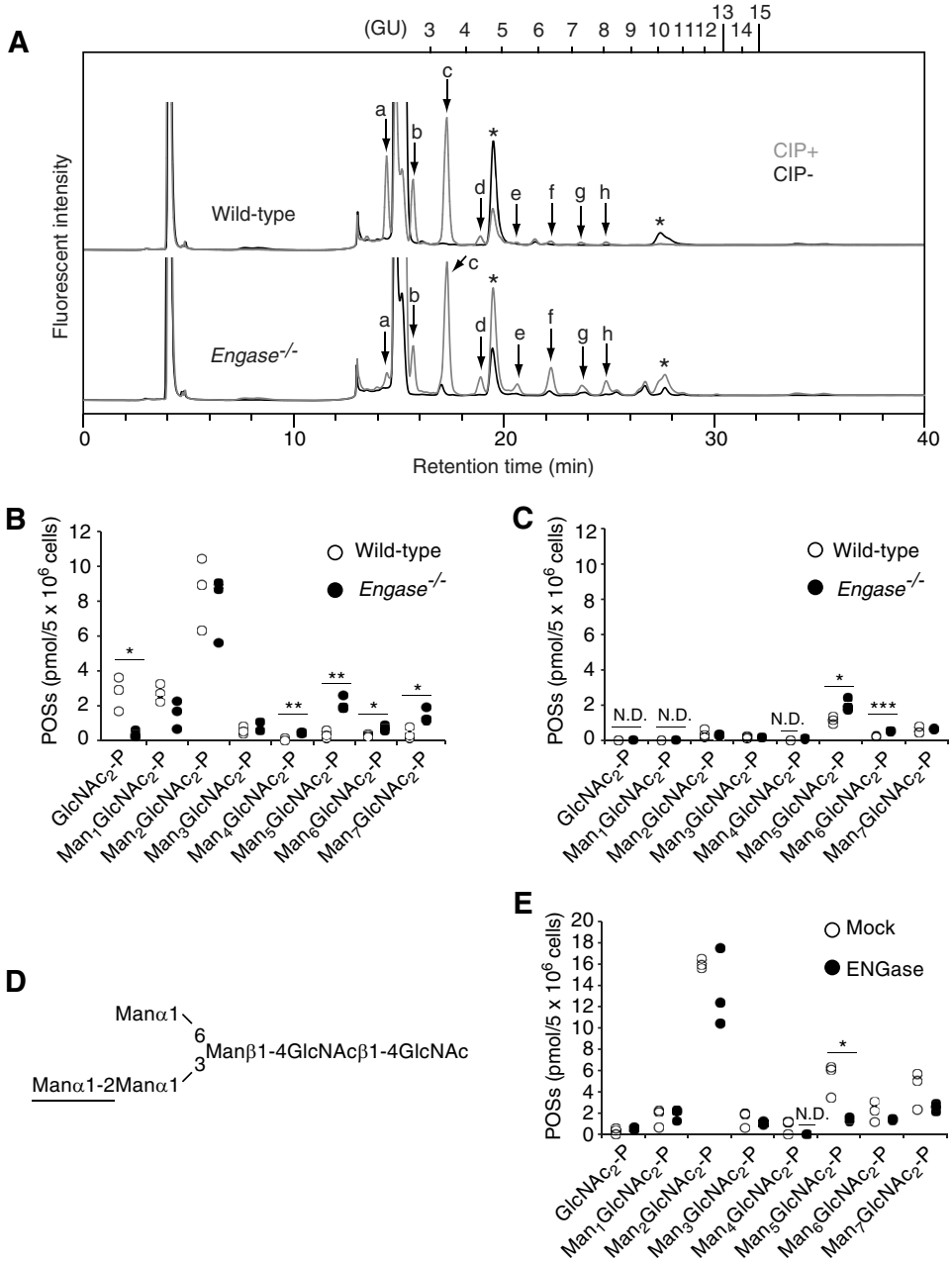

FIGURE 3. **POSs carrying a hexasaccharide accumulate in *Engase*$^{-/-}$ MEFs.** *A,* size-fractionation HPLC of POSs obtained from glucose-deprived wild-type (*top panel*) and *Engase*$^{-/-}$ (*bottom panel*) MEFs. POSs were treated with (+) or without (−) CIP and then fluorescently labeled. *Peaks a–h* were detected in a CIP-dependent manner. *Asterisks* indicate peaks derived from labeling reagents. PA-glucose oligomers (degree of polymerization = 3–15) were used as a reference, and the glucose units (*GU*) were represented on the HPLC chart. *B* and *C,* quantification of POSs obtained from MEFs cultured under low glucose (*B*) and normal glucose (*C*) conditions. Three independent experiments were carried out. *N.D.,* not detected. *, $p < 0.05$; **, $p < 0.005$; and ***, $p = 0.001$ (Student's *t* test). *D,* schematic representation of a hexasaccharide structure found in POSs that were increased in *Engase*$^{-/-}$ MEFs as compared with wild-type MEFs. An α1,2-linked Man residue important for the action of ENGase (32) is *underlined*. *E,* effects of ENGase overexpression in *Engase*$^{-/-}$ MEFs on POS catabolism. Three independent experiments were carried out. *N.D.,* not detected. *, $p = 0.013$ (Student's *t* test).

and further analyzed by dual-gradient reversed-phase HPLC (25) to determine their isomeric structures. In both glucose-deprived wild-type and *Engase*$^{-/-}$ MEFs, $Man_{0-7}GlcNAc_2$-P (Fig. 3*B*) were detected, and their glycan structures were identical to biosynthetic intermediates of DLOs (Table 2). Quantitative analyses of POSs showed that, in both glucose-deprived wild-type and *Engase*$^{-/-}$ MEFs, $Man_2GlcNAc_2$-P predominantly accumulated, and the knock-out of *Engase* did not markedly affect the amounts (Fig. 3*B*). Unexpectedly, however, the amounts of $GlcNAc_2$-P were significantly decreased in *Engase*$^{-/-}$ MEFs by an unclarified reason (Fig. 3*B*). By contrast, the amounts of $Man_{4-7}GlcNAc_2$-P were significantly increased in *Engase*$^{-/-}$ MEFs (Fig. 3*B*). A similar accumulation of $Man_{4-6}GlcNAc_2$-P was also observed in *Engase*$^{-/-}$ MEFs that were cultivated under normal glucose conditions (Fig. 3*C*), indicating that the availability of glucose is not a key factor in regulating the catabolism of $Man_{4-6}GlcNAc_2$-P. The glycan structures of POSs that significantly accumulated in *Engase*$^{-/-}$ MEFs were found to contain a hexasaccharide structure composed of Manα1,2Manα1,3(Manα1,6)Manβ1,4GlcNAcβ1,4GlcNAc

TABLE 2
Structures of POSs detected in wild-type and *Engase*$^{-/-}$ MEFs

Glycan ID[a] / Abbreviations	GUs[b]	Glycan isoforms	Structures of POSs[c]
a / $GlcNAc_2$-P	4.33	Gn2	GlcNAcβ1-4GlcNAc-P
b / $Man_1GlcNAc_2$-P	5.54	M1A	Manβ1-4GlcNAcβ1-4GlcNAc-P
c / $Man_2GlcNAc_2$-P	5.42	M2A	Manα1-3Manβ1-4GlcNAcβ1-4GlcNAc-P
d / $Man_3GlcNAc_2$-P	6.73	M3B	Manα1-6(Manα1-3)Manβ1-4GlcNAcβ1-4GlcNAc-P
e / $Man_4GlcNAc_2$-P	5.81	M4D	Manα1-2Manα1-3(Manα1-6)Manβ1-4GlcNAcβ1-4GlcNAc-P
f / $Man_5GlcNAc_2$-P	5.55	M5B	Manα1-2Manα1-2Manα1-3(Manα1-6)Manβ1-4GlcNAcβ1-4GlcNAc-P
g / $Man_6GlcNAc_2$-P	5.70	M6E	Manα1-2Manα1-2Manα1-3(Manα1-3Manα1-6)Manβ1-4GlcNAcβ1-4GlcNAc-P
h / $Man_7GlcNAc_2$-P	6.44	M7E	Manα1-2Manα1-3(Manα1-2Manα1-2Manα1-3(Manα1-6)Manβ1-4GlcNAcβ1-4GlcNAc-P

[a] Glycan ID was based on Fig. 3*A*.
[b] Elution positions of dephosphorylated, PA-labeled POSs were expressed as glucose units (GU) in dual-gradient reversed-phase HPLC (25).
[c] Glycan structures were deduced by dual-gradient reversed-phase HPLC using authentic glycan standards (25).

(Fig. 3*D*). To assess whether the accumulation of these POSs in *Engase*$^{-/-}$ MEFs is caused by the lack of ENGase, *Engase*$^{-/-}$ MEFs were transfected with a plasmid-encoding mouse *Engase*, and POSs that were accumulated in the transfected cells were quantitated. The overexpression of ENGase in *Engase*$^{-/-}$ MEFs resulted in a significant decrease in $Man_{4,5}GlcNAc_2$-P and showed a propensity for the reduction in $Man_{6,7}GlcNAc_2$-P (Fig. 3*E*). The partial reduction of these POSs by ENGase overexpression was most likely due to low transfection efficiencies in MEFs (~50% cells positive in the expression of green fluorescent protein used as a technical control; data not shown). All these results strongly indicate that ENGase is involved in the catabolism of POSs.

ENGase Hydrolyzes POSs in Vitro—Although our data clearly show that the lack of ENGase causes the accumulation of $Man_{4-7}GlcNAc_2$-P, the issue of whether ENGase catalyzes the hydrolysis of these POSs remained unknown. To address this issue, we carried out *in vitro* ENGase activity assays. First, we biochemically isolated DLOs with various glycan structures, *i.e.* $Man_3GlcNAc_2$, $Man_5GlcNAc_2$, $Man_9GlcNAc_2$, and $Glc_3Man_9GlcNAc_2$ (Fig. 4*A*, *left panels*), from various *S. cerevisiae* strains. POSs with various glycan structures ($Glc_3Man_9GlcNAc_2$-P, $Man_9GlcNAc_2$-P, $Man_5GlcNAc_2$-P, and $Man_3GlcNAc_2$-P) (Fig. 4*A*, *right panels*) were then prepared by incubating the DLO with the detergent-solubilized mouse liver microsomes, which contain DLO-pyrophosphatase activity (Fig. 4*B*). The POS preparations were fluorescently labeled only after treatment with alkaline phosphatase (Fig. 4*A*, *right panels, CIP+*), confirming that the reducing end of the POS preparations is phosphorylated.

In vitro ENGase assays using the POS preparations and the cytosolic fraction obtained from *Ngly1*$^{-/-}$ *Engase*$^{-/-}$ MEFs overexpressing ENGase showed that the order of hydrolytic rates of the POSs was $Glc_3Man_9GlcNAc_2$-P ≈ $Man_9GlcNAc_2$-

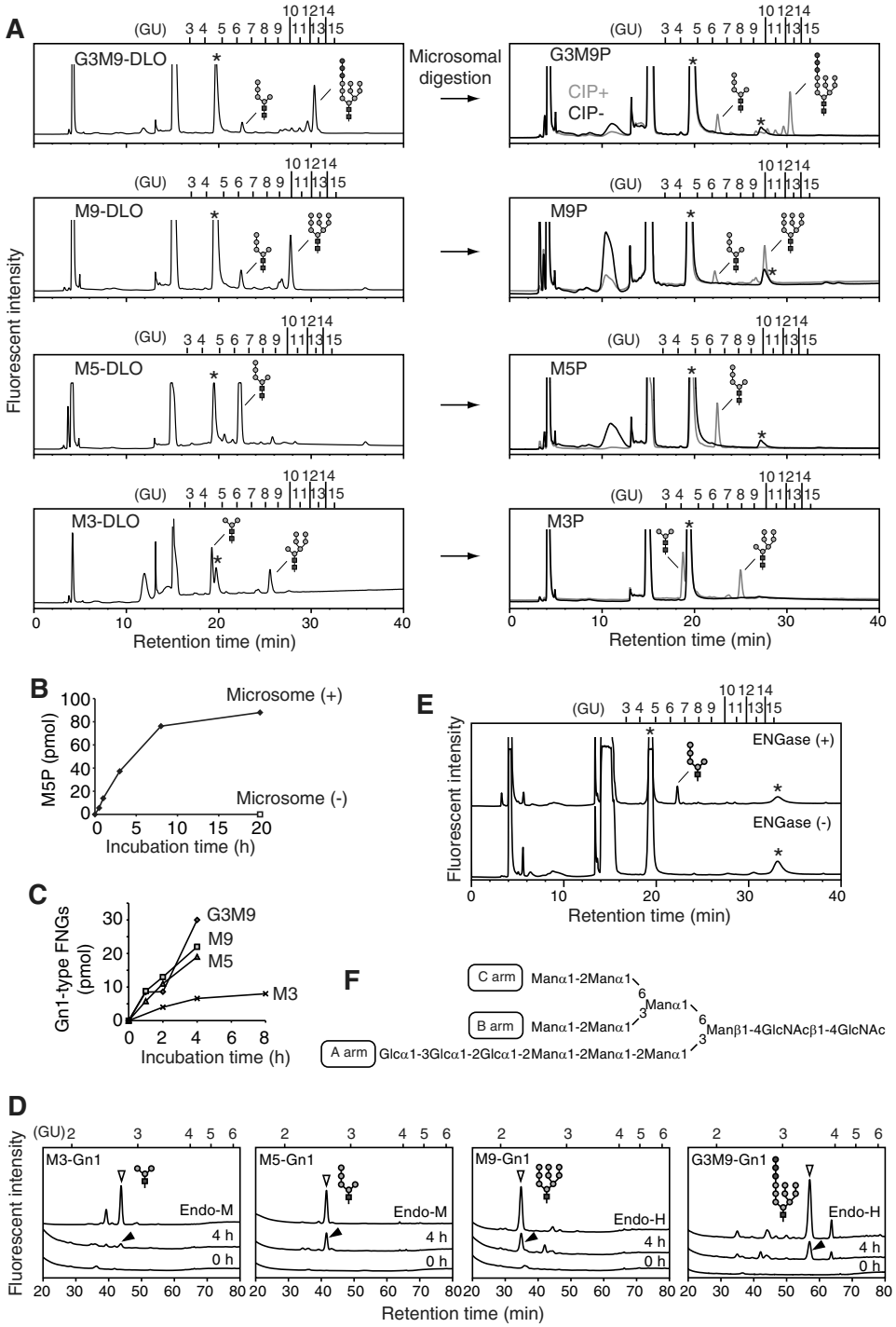

FIGURE 4. **ENGase hydrolyzes POSs *in vitro*.** *A,* size-fractionation HPLC profiles of DLOs extracted from wild-type ($Glc_3Man_9GlcNAc_2$-PP-dolichol; *G3M9-DLO*), *alg6*Δ ($Man_9GlcNAc_2$-PP-dolichol; *M9-DLO*), and *alg3*Δ ($Man_5GlcNAc_2$-PP-dolichol; *M5-DLO*) cells, which were transformed with a plasmid pRS425-GPD-ALG7 (15), and *alg11*Δ cells ($Man_3GlcNAc_2$-PP-dolichol; *M3-DLO*) (*left panels*). The glycan structures shown in the HPLC charts were deduced based on previously reported data (36–41) and further confirmed by the product analyses in the ENGase assay (Table 3). The DLOs were digested with mouse liver microsomes (*microsomal digestion*) to obtain POSs (*G3M9P, M9P, M5P,* and *M3P*, *right panels*). The resulting POSs were treated with (+) or without (−) CIP before fluorescent labeling. *B,* time course analysis of the DLO-pyrophosphatase assay in the presence (+) or absence (−) of microsomes using M5P as a substrate. *C,* time course analyses of the ENGase assay using M3P, M5P, M9P. and G3M9P as substrates. The amounts of Gn1-type FNGs were quantitated by size-fractionation HPLC. *D,* product analyses for the ENGase assay by dual-gradient reversed-phase HPLC. *White arrowheads* indicate the elution positions of authentic Gn1-type FNGs generated by Endo-H or Endo-M digestion of POSs. *Black arrowheads* indicate peaks that are generated by ENGase and co-eluted with the authentic standard glycans. Unassigned peaks generated by endoglycosidase digestions are probably derived from POSs that were co-purified with G3M9P, M9P, M5P, and M3P (see also *A*, *right panels*). *E,* ENGase assay using M5P as a substrate and the cytosolic fraction obtained from either ENGase-transfected (+) or non-transfected (−) *Ngly1*$^{-/-}$ *Engase*$^{-/-}$ MEFs as an enzyme source. The reaction mixtures were analyzed by size-fractionation HPLC. *F,* schematic representation of $Glc_3Man_9GlcNAc_2$ glycan. The position of the *A, B,* and *C arms* of the glycan are indicated. *Asterisks* in *A* and *E* indicate peaks derived from labeling reagents. PA-glucose oligomers (degree of polymerization = 3–15) was used as a reference, and the glucose units (*GU*) are represented on the HPLC chart.

TABLE 3
***In vitro* ENGase activity assay using POSs with various glycan structures**

Structures of POSs used as substrates	Structures of reaction products (GUs)[a]	Hydrolytic rates (pmol/h)[b]	Relative activity[c]
$Glc_3Man_9GlcNAc_2$-P	$Glc_3Man_9GlcNAc_1$ (3.50)	8.5	0.9
$Man_9GlcNAc_2$-P	$Man_9GlcNAc_1$ (2.32)	8.8	1.0
$Man_5GlcNAc_2$-P	$Man_5GlcNAc_1$ (2.65)	5.8	0.6
$Man_3GlcNAc_2$-P	$Man_3GlcNAc_1$ (2.76)	2.0	0.2

[a] Glycan structures were determined by the elution positions of both size-fractionation and dual-gradient reversed-phase HPLC and comparison with authentic standard glycans (25). To verify the position of Gn1-type FNGs under the HPLC conditions used, the reaction products were analyzed in parallel with POSs that were digested with Endo-H (for $Glc_3Man_9GlcNAc_2$-P and $Man_9GlcNAc_2$-P) or Endo-M ($Man_5GlcNAc_2$-P and $Man_3GlcNAc_2$-P).
[b] The amounts of reaction products were estimated from peak area of PA-Glc_6 in size-fractionation HPLC. The hydrolytic rates were estimated based on the amounts of Gn1-type FNGs at 1 h ($Glc_3Man_9GlcNAc_1$, $Man_9GlcNAc_1$, and $Man_5GlcNAc_1$) and 2 h ($Man_3GlcNAc_1$) after incubation.
[c] Hydrolytic rates of $Man_9GlcNAc_2$-P were set to 1.0.

$p >$ $Man_5GlcNAc_2$-P $\gg$ $Man_3GlcNAc_2$-P (Fig. 4*C* and Table 3). Dual-gradient reversed-phase HPLC analysis (25) of the reaction mixtures confirmed the generation of Gn1-type FNGs, *i.e.* $Glc_3Man_9GlcNAc_1$, $Man_9GlcNAc_1$, $Man_5GlcNAc_1$, and $Man_3GlcNAc_1$ (Fig. 4*D* and Table 3). When the cytosolic fraction obtained from non-transfected *Ngly1*$^{-/-}$ *Engase*$^{-/-}$ MEFs was used, no hydrolysis of $Man_5GlcNAc_2$-P was detected (Fig. 4*E*), verifying that the cytosolic fraction of the non-transfected *Ngly1*$^{-/-}$ *Engase*$^{-/-}$ MEFs is devoid of degradation activity for POSs. Therefore, our assay system using the cytosol fraction of the ENGase-overexpressing *Ngly1*$^{-/-}$ *Engase*$^{-/-}$ MEFs is a reliable one, especially when appropriate glycosidase inhibitors (swainsonine, kifunensine, and castanospermine) are included in the reaction mixture to prevent the glycan trimming of reaction products during the incubation (see "Experimental Procedures" for the detailed conditions). All these results indicate that, although ENGase has a broad substrate specificity for POSs, the presence of α1,2-linked mannose residues at the A arm (Fig. 4*F*), as well as a branching structure at the B and C arms, facilitates the action of this enzyme.

Discussion

A putative DLO-degrading enzyme has been implicated in the production of POSs (11), whereas the precise cleavage site of DLOs by this enzyme has not been unequivocally determined. Our LC-MS analyses of intact POSs showed that one phosphate group is present (Fig. 2) at the reducing end of POSs (Fig. 3*A*) (10, 13), providing conclusive evidence that the putative DLO-degrading enzyme is a DLO-pyrophosphatase that splits the pyrophosphate bond of DLOs producing mono-phosphorylated POSs. Although mono-phosphorylated POSs have been identified by MS in bacteria (30) or in milk oligosaccharides (31), to the best of our knowledge this is the first example of the use of MS for the identification of DLO-derived POSs of mammalian origin.

In vitro DLO-pyrophosphatase assays revealed that the enzyme exhibits broad substrate specificities for glycan structures (Fig. 4*A*, *right panels*), and even the fully assembled DLO ($Glc_3Man_9GlcNAc_2$-PP-Dol) can be a substrate *in vitro*. This result raises the issue of why only limited POS structures, *i.e.* $Man_{0-7}GlcNAc_2$-P, were detected in MEFs (Fig. 3, *B* and *C*) (10, 13). These POSs are produced from both the cytosolic and luminal species of DLOs, which negligibly accumulate in MEFs (10). By contrast, $Glc_3Man_9GlcNAc_2$-PP-Dol is the predominant DLO at the steady state in MEFs (10), whereas little $Glc_3Man_9GlcNAc_2$-P is detected even in *Engase*$^{-/-}$ MEFs (Fig. 3, *B* and *C*). Our findings thus imply that the accessibility of the DLO-pyrophosphatase to the fully assembled DLO is somehow limited *in vivo* via unknown mechanisms. Although it is also possible that the glycan trimming of large POSs by glycosidases may generate small POSs from large POSs, such as $Glc_3Man_9GlcNAc_2$-P, previous studies have shown that glycan structures of POSs are barely altered by treatment with various glycosidase inhibitors, such as castanospermine (13), kifunensine (13), and swainsonine (10, 13), suggesting that such a possibility is unlikely. Irrespective of mechanisms involved, the identification of the membrane topology of the catalytic site(s) of the DLO-pyrophosphatase will provide deeper insights into important aspects of the regulation of the action of DLO-pyrophosphatase *in vivo*.

Our data showed that large POSs, *i.e.* $Man_{4-7}GlcNAc_2$-P, carrying the Manα1,2Manα1,3(Manα1,6)Manβ1,4GlcNAcβ1,4GlcNAc structure tend to accumulate in *Engase*$^{-/-}$ MEFs (Fig. 3, *B* and *C*). The accumulation of these POSs in *Engase*$^{-/-}$ MEFs is consistent with the finding that, *in vitro*, ENGase efficiently hydrolyzes POSs bearing α1,2-linked mannose residues located at the A arm (Table 3). In contrast, ENGase hydrolyzes $Man_3GlcNAc_2$-P at much slower rates (Table 3). The substrate specificity of ENGase is consistent with the previous report showing that glycans that contain a Manα1,2Manα1,3Manβ1,4GlcNAcβ1,4GlcNAc structure serve as good substrates of ENGase (32). These findings can explain, at least in part, the reason why $Man_{0-3}GlcNAc_2$-P accumulates to a lesser extent

when compared with the larger POSs in *Engase*$^{-/-}$ MEFs. The glycan processing of POSs by ENGase is of biological relevance, because the putative FNG transporter that resides in the lysosomal membrane does not directly transport POSs into lysosomes (33). Therefore, the ENGase-mediated processing of POSs plays a crucial role in initiating their cytosolic clearance.

We noted that the levels of $GlcNAc_2$-P were significantly reduced in *Engase*$^{-/-}$ MEFs, raising the possibility that the biosynthesis of $GlcNAc_2$-PP-Dol is also compromised in glucose-deprived *Engase*$^{-/-}$ MEFs. The action of ENGase produces free GlcNAc and GlcNAc-1-P from Gn2-type FNGs and POSs, respectively (Fig. 1). These sugars may be recycled for the biosynthesis of UDP-GlcNAc, which is an essential sugar donor substrate for the assembly of $GlcNAc_2$-PP-Dol. It is also possible that the catabolism of $GlcNAc_2$-P is enhanced in the absence of ENGase. In this regard, it remains to be clarified how small POSs, which are poor substrates of ENGase, are catabolized. A putative POS-phosphatase activity was reported in the microsome fraction from human liver (14), but the molecular nature of this phosphatase is currently unknown. Moreover, we previously found that the induction of bulk autophagy by amino acid starvation reduces the levels of FNGs in the cytosol (34). Further studies will be needed to elucidate the molecular mechanism involved in the catabolism of small POSs.

In summary, the above findings demonstrate that POSs are mono-phosphorylated, thereby implicating the action of a DLO-pyrophosphatase in their production. Moreover, we identified the cytosolic ENGase as a POS-catabolizing enzyme that preferentially hydrolyzes POSs carrying the Manα1,2Manα1,3(Manα1,6)Manβ1,4GlcNAcβ1,4GlcNAc structure. This study provides mechanistic insights into the generation and the catabolism of POSs in mammalian cells.

Author Contributions—Y. H. and T. S. designed the study. Y. H. prepared the samples used for Fig. 2 and also performed the experiments for Figs. 3 and 4 and Tables 2 and 3. C. H. performed the experiments for Figs. 4, *C–E,* and Table 3. S. Y. and N. D. performed the analyses shown in Fig. 2. Y. H. and T. S. analyzed all the data and wrote the manuscript. All authors reviewed the results and approved the final version of the manuscript.

Acknowledgments—We thank our laboratory members for fruitful discussions.

References

1. Kelleher, D. J., and Gilmore, R. (2006) An evolving view of the eukaryotic oligosaccharyltransferase. *Glycobiology* **16,** 47R–62R
2. Harada, Y., Hirayama, H., and Suzuki, T. (2015) Generation and degradation of free asparagine-linked glycans. *Cell. Mol. Life Sci.* **72,** 2509–2533
3. Shrimal, S., Cherepanova, N. A., and Gilmore, R. (2015) Cotranslational and posttranslocational *N*-glycosylation of proteins in the endoplasmic reticulum. *Semin. Cell Dev. Biol.* **41,** 71–78
4. Doerrler, W. T., and Lehrman, M. A. (1999) Regulation of the dolichol pathway in human fibroblasts by the endoplasmic reticulum unfolded protein response. *Proc. Natl. Acad. Sci. U.S.A.* **96,** 13050–13055
5. Baumann, H., and Jahreis, G. P. (1983) Glucose starvation leads in rat hepatoma cells to partially *N*-glycosylated glycoproteins including α1-acid glycoproteins. Identification by endoglycolytic digestions in polyacrylamide gels. *J. Biol. Chem.* **258,** 3942–3949
6. Turco, S. J., and Pickard, J. L. (1982) Altered G-protein glycosylation in vesicular stomatitis virus-infected glucose-deprived baby hamster kidney cells. *J. Biol. Chem.* **257,** 8674–8679
7. Rearick, J. I., Chapman, A., and Kornfeld, S. (1981) Glucose starvation alters lipid-linked oligosaccharide biosynthesis in Chinese hamster ovary cells. *J. Biol. Chem.* **256,** 6255–6261
8. Gershman, H., and Robbins, P. W. (1981) Transitory effects of glucose starvation on the synthesis of dolichol-linked oligosaccharides in mammalian cells. *J. Biol. Chem.* **256,** 7774–7780
9. Gao, N., Shang, J., and Lehrman, M. A. (2005) Analysis of glycosylation in CDG-Ia fibroblasts by fluorophore-assisted carbohydrate electrophoresis: implications for extracellular glucose and intracellular mannose 6-phosphate. *J. Biol. Chem.* **280,** 17901–17909
10. Harada, Y., Nakajima, K., Masahara-Negishi, Y., Freeze, H. H., Angata, T., Taniguchi, N., and Suzuki, T. (2013) Metabolically programmed quality control system for dolichol-linked oligosaccharides. *Proc. Natl. Acad. Sci. U.S.A.* **110,** 19366–19371
11. Cacan, R., Hoflack, B., and Verbert, A. (1980) Fate of oligosaccharide-lipid intermediates synthesized by resting rat-spleen lymphocytes. *Eur. J. Biochem.* **106,** 473–479
12. Belard, M., Cacan, R., and Verbert, A. (1988) Characterization of an oligosaccharide-pyrophosphodolichol pyrophosphatase activity in yeast. *Biochem. J.* **255,** 235–242
13. Peric, D., Durrant-Arico, C., Delenda, C., Dupré, T., De Lonlay, P., de Baulny, H. O., Pelatan, C., Bader-Meunier, B., Danos, O., Chantret, I., and Moore, S. E. (2010) The compartmentalisation of phosphorylated free oligosaccharides in cells from a CDG Ig patient reveals a novel ER-to-cytosol translocation process. *PLoS ONE* **5,** e11675
14. Vleugels, W., Duvet, S., Peanne, R., Mir, A. M., Cacan, R., Michalski, J. C., Matthijs, G., and Foulquier, F. (2011) Identification of phosphorylated oligosaccharides in cells of patients with a congenital disorders of glycosylation (CDG-I). *Biochimie* **93,** 823–833
15. Harada, Y., Buser, R., Ngwa, E. M., Hirayama, H., Aebi, M., and Suzuki, T. (2013) Eukaryotic oligosaccharyltransferase generates free oligosaccharides during *N*-glycosylation. *J. Biol. Chem.* **288,** 32673–32684
16. Harada, Y., Masahara-Negishi, Y., and Suzuki, T. (2015) Cytosolic-free oligosaccharides are predominantly generated by the degradation of dolichol-linked oligosaccharides in mammalian cells. *Glycobiology* **25,** 1196–1205
17. Suzuki, T. (2015) The cytoplasmic peptide:*N*-glycanase (Ngly1)–basic science encounters a human genetic disorder. *J. Biochem.* **157,** 23–34
18. Hirayama, H., Hosomi, A., and Suzuki, T. (2015) Physiological and molecular functions of the cytosolic peptide:*N*-glycanase. *Semin. Cell Dev. Biol.* **41,** 110–120
19. Suzuki, T., Yano, K., Sugimoto, S., Kitajima, K., Lennarz, W. J., Inoue, S., Inoue, Y., and Emori, Y. (2002) Endo-β-*N*-acetylglucosaminidase, an enzyme involved in processing of free oligosaccharides in the cytosol. *Proc. Natl. Acad. Sci. U.S.A.* **99,** 9691–9696
20. Kato, T., Fujita, K., Takeuchi, M., Kobayashi, K., Natsuka, S., Ikura, K., Kumagai, H., and Yamamoto, K. (2002) Identification of an endo-β-*N*-acetylglucosaminidase gene in *Caenorhabditis elegans* and its expression in *Escherichia coli*. *Glycobiology* **12,** 581–587
21. Chantret, I., Fasseu, M., Zaoui, K., Le Bizec, C., Sadou Yayé, H., Dupré, T., and Moore, S. E. (2010) Identification of roles for peptide: *N*-glycanase and endo-β-*N*-acetylglucosaminidase (Engase1p) during protein *N*-glycosylation in human HepG2 cells. *PLoS ONE* **5,** e11734
22. Suzuki, T., Hara, I., Nakano, M., Shigeta, M., Nakagawa, T., Kondo, A., Funakoshi, Y., and Taniguchi, N. (2006) Man2C1, an α-mannosidase, is involved in the trimming of free oligosaccharides in the cytosol. *Biochem. J.* **400,** 33–41
23. Saint-Pol, A., Bauvy, C., Codogno, P., and Moore, S. E. (1997) Transfer of free polymannose-type oligosaccharides from the cytosol to lysosomes in cultured human hepatocellular carcinoma HepG2 cells. *J. Cell Biol.* **136,** 45–59
24. Huang, C., Harada, Y., Hosomi, A., Masahara-Negishi, Y., Seino, J., Fujihira, H., Funakoshi, Y., Suzuki, T., Dohmae, N., and Suzuki, T. (2015) Endo-β-*N*-acetylglucosaminidase forms N-GlcNAc protein aggregates during ER-associated degradation in Ngly1-defective cells. *Proc. Natl. Acad. Sci. U.S.A.* **112,** 1398–1403

25. Suzuki, T., Matsuo, I., Totani, K., Funayama, S., Seino, J., Taniguchi, N., Ito, Y., and Hase, S. (2008) Dual-gradient high-performance liquid chromatography for identification of cytosolic high-mannose-type free glycans. *Anal. Biochem.* **381,** 224–232
26. Rose, M. D., Winston, F., and Hieter, P. (1990) *Methods in Yeast Genetics*, Cold Spring Harbor Laboratory Press, Cold Spring Harbor, NY
27. Haga, Y., Totani, K., Ito, Y., and Suzuki, T. (2009) Establishment of a real-time analytical method for free oligosaccharide transport from the ER to the cytosol. *Glycobiology* **19,** 987–994
28. Hirayama, H., Seino, J., Kitajima, T., Jigami, Y., and Suzuki, T. (2010) Free oligosaccharides to monitor glycoprotein endoplasmic reticulum-associated degradation in *Saccharomyces cerevisiae*. *J. Biol. Chem.* **285,** 12390–12404
29. Hase, S., Ikenaka, T., and Matsushima, Y. (1979) Analyses of oligosaccharides by tagging the reducing end with a fluorescent compound. I. Application to glycoproteins. *J. Biochem.* **85,** 989–994
30. Dwivedi, R., Nothaft, H., Reiz, B., Whittal, R. M., and Szymanski, C. M. (2013) Generation of free oligosaccharides from bacterial protein *N*-linked glycosylation systems. *Biopolymers* **99,** 772–783
31. Albrecht, S., Lane, J. A., Mariño, K., Al Busadah, K. A., Carrington, S. D., Hickey, R. M., and Rudd, P. M. (2014) A comparative study of free oligosaccharides in the milk of domestic animals. *Br. J. Nutr.* **111,** 1313–1328
32. Kato, T., Hatanaka, K., Mega, T., and Hase, S. (1997) Purification and characterization of endo-β-*N*-acetylglucosaminidase from hen oviduct. *J. Biochem.* **122,** 1167–1173
33. Saint-Pol, A., Codogno, P., and Moore, S. E. (1999) Cytosol-to-lysosome transport of free polymannose-type oligosaccharides. Kinetic and specificity studies using rat liver lysosomes. *J. Biol. Chem.* **274,** 13547–13555
34. Seino, J., Wang, L., Harada, Y., Huang, C., Ishii, K., Mizushima, N., and Suzuki, T. (2013) Basal autophagy is required for the efficient catabolism of sialyloligosaccharides. *J. Biol. Chem.* **288,** 26898–26907
35. Suzuki, T., and Harada, Y. (2014) Non-lysosomal degradation pathway for *N*-linked glycans and dolichol-linked oligosaccharides. *Biochem. Biophys. Res. Commun.* **453,** 213–219
36. Reiss, G., te Heesen, S., Zimmerman, J., Robbins, P. W., and Aebi, M. (1996) Isolation of the ALG6 locus of *Saccharomyces cerevisiae* required for glucosylation in the *N*-linked glycosylation pathway. *Glycobiology* **6,** 493–498
37. Aebi, M., Gassenhuber, J., Domdey, H., and te Heesen, S. (1996) Cloning and characterization of the ALG3 gene of *Saccharomyces cerevisiae*. *Glycobiology* **6,** 439–444
38. Cipollo, J. F., Trimble, R. B., Chi, J. H., Yan, Q., and Dean, N. (2001) The yeast ALG11 gene specifies addition of the terminal α,2-Man to the Man5GlcNAc2-PP-dolichol *N*-glycosylation intermediate formed on the cytosolic side of the endoplasmic reticulum. *J. Biol. Chem.* **276,** 21828–21840
39. Helenius, J., Ng, D. T., Marolda, C. L., Walter, P., Valvano, M. A., and Aebi, M. (2002) Translocation of lipid-linked oligosaccharides across the ER membrane requires Rft1 protein. *Nature* **415,** 447–450
40. Absmanner, B., Schmeiser, V., Kämpf, M., and Lehle, L. (2010) Biochemical characterization, membrane association and identification of amino acids essential for the function of Alg11 from *Saccharomyces cerevisiae*, an α1,2-mannosyltransferase catalysing two sequential glycosylation steps in the formation of the lipid-linked core oligosaccharide. *Biochem. J.* **426,** 205–217
41. Huffaker, T. C., and Robbins, P. W. (1983) Yeast mutants deficient in protein glycosylation. *Proc. Natl. Acad. Sci. U.S.A.* **80,** 7466–7470